The ASM Report System

Low Cycle Fatigue of Ti-6Al-4V Alloy

S. A. Sattar
D. H. Kellogg
H. J. Oberle
B. N. Greene

Presented at the 1968 Materials
Engineering Exposition & Congress
14-17 October 1968
Detroit, Michigan

AMERICAN SOCIETY FOR METALS
METALS PARK, OHIO

TECHNICAL
REPORT NO. D 8-24.4

$3 per copy
$1.50 to ASM Members

Low Cycle Fatigue Investigation of Titanium 6Al-4V Alloy

S.A. Sattar, H.J. Oberle, D.H. Kellogg and B.N. Greene

To evaluate the effect of forging and heat treatment parameters on titanium 6Al-4V alloy (AMS 4928), various microstructures were investigated and compared in a deflection-controlled low cycle fatigue test program. The test specimen was designed to simulate the strain state observed in gas turbine engine components. The results of this study will be used to optimize the design of compressor disks. Parameters investigated include environment, mean strain, and surface condition. The number of cycles to initiate a fatigue crack and the rate of crack propagation were measured to evaluate the microstructures. The number of cycles to crack initiation was correlated with a mechanistic theory based on the static properties of the materials investigated.

The authors are associated with the Pratt and Whitney Aircraft, Division of United Aircraft Inc., East Hartford, Connecticut. This paper is scheduled for the Fabrication and Properties of Metals session of the National Metal Congress, 1968, Detroit.

Introduction

The most widely used titanium alloy for gas turbine engine compressor disk application is Ti-6Al-4V. This alloy offers a 50 to 60% improvement in strength-to-weight ratio compared with steel and possesses good fracture toughness. In order to more completely characterize the alloy for use in future high performance gas turbine engines, a comprehensive program was initiated to evaluate the effect of variation of processing variables on mechanical properties. Of primary interest were the effects of these variables on low cycle fatigue and fracture toughness behavior and on susceptibility to aqueous salt stress corrosion.

Static tensile, load-controlled low cycle fatigue and fracture toughness data were obtained as background information on three processed microstructures - transformed beta, 10% primary alpha and 50% primary alpha. The principal part of the program involved an investigation of parameters such as environment, surface finish and strain level on the deflection-controlled low cycle fatigue performance of the various microstructures. This included an evaluation of both crack initiation and crack propagation behavior. Analytical and mechanistic approaches to the problem of low cycle fatigue in Ti-6Al-4V were explored. These factors are discussed in detail.

Procedure

Processing History. Twelve compressor disk forgings of Ti-6Al-4V were processed to three different microstructures by forging and heat treating at various temperatures. Forging was carried out in a two-step block and finish hammer forge operation. The disks containing primary alpha were forged in the two-phase alpha-beta field while the beta-forged disks were worked in the single-phase beta region. All forgings were conventionally solution treated in the two-phase alpha-beta region and aged at 1300F for two hours to give the microstructures, 10% primary alpha, 50% primary alpha, and transformed beta shown in Figure 1. The processing variables used to obtain these microstructures are given in Table I along with the chemical composition of the forging billets. Specimens machined from forgings were used to determine the tensile, low cycle fatigue, and fracture toughness properties of the three microstructures.

Preliminary Materials Evaluation. Tensile tests at 70°F showed that the beta-forged material has lower strength and ductility than those materials which have microstructures containing equiaxed primary alpha. The tensile data of the three materials are shown in Table II.

Fracture toughness evaluation of the three microstructures in air was conducted on pre-cracked notched bend specimens. The specimen configuration is shown in Figure 2. The plane strain fracture toughness, K_{IC}, for the four-point loaded specimens is shown in Table II. The load P was determined either at "pop-in" or where the load deflection curve deviated from linearity.

Load-controlled low cycle fatigue tests were performed on notched (K_t2) 0.250-inch-diameter specimens. The specimens were cycled axially in the 0 to 100 ksi stress range at a rate of 12 cycles per minute. Prior to testing the specimens were stress relieved and glass-bead peened.

Cycles to crack initiation and to failure are shown in Table III. Results from these tests did not show conclusively the superior fatigue performance of any one material.

Strain-Controlled Low Cycle Fatigue. Based on the preliminary evaluation, a strain-controlled low cycle fatigue test program using a specially designed specimen was conducted to more completely evaluate the low cycle fatigue performance of the three microstructures. A one-half-inch-diameter bolt hole was machined in a block 2-1/2" x 1-1/2" x 1-1/4" with the hole axis in the direction of the 1-1/2" dimension. The hole was drilled, bored, honed and polished according to a procedure typical of production operations as shown in Table IV. The block was cut to yield two identical test specimens as shown in Figure 3.

The test apparatus was designed to apply a cyclic load resulting in a controlled-bending strain between fixed deflection limits. A photograph of the test rig and the specimen is shown in Figure 4. The specimen design and the applied load result in a strain at the root of the test specimen bolt hole closely approximating that present at bolt holes in a turbine engine compressor disk. Figure 5 shows that the calculated strains present in the bending specimen and a hole in a rotating disk are comparable in the area of interest. Additional reasons for the choice of specimen design are as follows:

1) Low cycle fatigue crack propagation studies of titanium alloys have been carried out by other researchers (1, 2) utilizing a bending specimen under constant strain. This specimen geometry and loading would allow comparison with these studies.

2) Crack initiation is easily observed and crack propagation can be readily followed and accurately measured.

3) A small volume of material and simple geometry result in a relatively inexpensive specimen. At the same time, all appropriate production finish operations can be incorporated.

4) The specimen readily adapts to constant deflection testing and duplication of a wide range of strain levels with moderate load application.

5) The specimen can be easily notched by electric discharge machining (EDM) techniques for low cycle fatigue crack growth rate studies.

Disadvantages are that no fracture toughness measurements can be made on this type of geometry and that realistic crack propagation data cannot be studied after a crack length of approximately 1/2 inch is attained.

To accomplish the objectives of this phase of the program, specimens of each microstructure were strain cycled at a rate of 12 cycles per minute and inspected at 1000 cycle intervals using a fluorescent penetrant inspection technique. Cycles to crack initiation were determined in this manner.

To insure crack propagation from a single origin, propagation data were obtained from specimens notched at the hole center position by the EDM method. Notch size was approximately 0.005 in. in diameter and 0.008 in. deep. Crack propagation data were obtained at 500 cycle intervals using replicating techniques while the specimens were subjected to 0.3% tensile strain. Crack lengths were measured from the replicas under 100X magnification. The replication technique affords an accurate and permanent record of the propagating crack.

p7

Results

Crack Initiation. Of the three microstructures studied, the beta-forged material was the least resistant to crack initiation. This result is based on specimens taken from six disks processed in the manner previously specified. The number of cycles to crack initiation are shown in Table V and illustrated in the bar graph of Figure 6. Crack initiation in the beta-forged material occurred between 2000 and 4000 cycles whereas crack initiation in the two-phase forged material occurred between 4000 and 16,000 cycles.

Figure 8 shows the predicted low cycle fatigue curve based on a mechanistic theory using the static tensile properties. Initiation lives of 2000 cycles for the beta forged, and 4000 cycles for the alpha-beta forged titanium were obtained for a strain range of 0 - 0.9%.

The data obtained for glass-bead peened specimens were in the same range as those obtained for as-machined specimens. The crack initiation resistance of beta-forged material relative to two-phase forged material remained the same. However, Figure 7 shows that the data from glass-bead peened specimens have significantly narrower scatter bands than data from as-machined specimens. The minimum initiation life is raised from 2000 to 4000 cycles for beta-forged material and from 4000 to 8000 cycles for alpha-beta forged material.

Crack Propagation. Testing of EDM notched specimens showed that the crack propagation rates in air, measured from plastic replicas, were nearly the same for all microstructures tested as shown in Figure 9 and in Table V. Crack propagation occurs in two stages. The first stage is characterized by a slow propagation rate of the order of 10 micro-inches/cycle. The transition between the first and the second crack propagation stages occurs at about 0.035 in., and the growth rate increases to approximately 140 microinches/cycle until the crack extends the length of the bolt hole surface.

Crack propagation tests run in artificial sea water failed to show differences in behavior among the microstructures tested. The shape of the curve depicting crack length vs. number of cycles is similar to those obtained from comparable tests in air. However, crack propagation is more rapid in artificial sea water than in air in both stages of crack propagation. Figure 10 shows the crack extension in sea water as a function of the number of test cycles. Crack growth rates listed in Table VI show that artificial sea water increases the first stage growth rate from approximately 10 microinches/cycle in air to approximately 20 microinches/cycle. Second stage crack growth rate is increased from approximately 140 microinches/cycle to approximately 440 microinches/cycle.

EDM notched specimens were also cycled about zero mean strain between ±0.45% strain limits to observe the effect of mean strain on crack propagation. The crack advanced in a manner similar to that observed for specimens tested in the 0 to 0.9% strain range. First stage crack propagation rates were approximately 1.4 microinches per cycle, an order of magnitude lower than that for the propagation specimens tested in the 0 to 0.9% strain range. Second stage growth rates were approximately 24 microinches/cycle. These results are shown in Figure 2 and crack propagation rates are listed in Table VI. No significant difference in crack propagation resistance among the

candidate microstructures was observed in either stage of crack growth. To determine the effect of compressive residual surface stresses on crack propagation, three EDM notched specimens were glass-bead peened and compared with a series of specimens with as-machined surfaces taken from the same forging. The crack propagation curves shown in Figure 12 indicate that glass-bead peening does not significantly affect crack propagation. The crack propagation data for specimens with both as-machined and glass-bead peened surfaces are listed in Table VI.

Discussion

Crack Initiation. The lower crack initiation resistance of beta-forged Ti-6Al-4V cannot be ascribed to any single factor. Beta-forged material is weaker and less ductile than two-phase forged material, which could explain the reduction in the crack initiation life. Wells and Sullivan (3) have shown that crack initiation occurs primarily in slip bands but also occurs at phase boundaries. Beta-forged material, because of its lower proportional limit, is more subject to slip band formation. The needle-like nature of the primary alpha in beta-forged Ti-6Al-4V also provides a greater percentage of phase boundary on any planar section. This creates an increased number of potential initiation sites for beta-forged material.

Previous researchers (4-7) have shown that the low cycle fatigue behavior of materials can be predicted by methods utilizing ductility, ultimate strength and endurance strength. First, consider that the total strain range is the sum of both plastic and elastic components,

$$\epsilon_T = \epsilon_p + \epsilon_e \qquad (1)$$

where
ϵ_T = total strain range
ϵ_p = plastic strain range
ϵ_e = elastic strain range

The plastic strain portion of this equation is dependent on the fracture ductility and has been modified to include the mean strain whose effect is considered a condition of prestrain and can be expressed as

$$N = \left(\frac{\epsilon_f - \epsilon_m}{\epsilon_T} \right)^2 \qquad (2)$$

where
N = cycles to failure
ϵ_f = fracture strain
$\epsilon_m = 1/2\ (\epsilon_{max} - \epsilon_{min})$ = mean strain
ϵ_T = total strain range

Equation (2) can be rewritten as:

$$\epsilon_T = \frac{\epsilon_f - \epsilon_m}{N^{1/2}} \qquad (3)$$

For a low number of cycles $\epsilon_T = \epsilon_p$ since the elastic component of strain is small compared to the plastic component. Determination of the elastic component can be made by drawing the following points:

1) At 1/4 cycle, the elastic strain range can be estimated as approximately σuts/E where σuts is the ultimate tensile strength and E is the elastic modulus.

2) At 10^8 cycles, the elastic strain range can be estimated as approximately σe/E where σe is the endurance strength of the material.

The elastic portion of the fatigue curve is interpolated as a straight line on a log-log scale and can be expressed by the following relationship:

$$\epsilon_e = \frac{\sigma_{UTS}}{E} (4N)^{\frac{\ln \sigma_{UTS}/\sigma_e}{\ln(.25 \times 10^{-8})}} \qquad (4)$$

Substitution of Equations (3) and (4) into Equation (1) yields the equation of the low cycle fatigue curve,

$$\epsilon_T = \frac{\epsilon_f - \epsilon_M}{N^{1/2}} + \frac{\sigma_{UTS}}{E} (4N)^{\frac{\ln \sigma_{UTS}/\sigma_e}{\ln(.25 \times 10^{-8})}} \qquad (5)$$

This equation is represented by the curves in Figure 8 for both beta-forged and alpha-beta forged material. The experimental data reported in Table V for a strain range of 0 to 0.9% shows good agreement with these curves.

Crack Propagation. The absence of any perceptible effect of microstructure on crack propagation indicates that the observed differences in ductility and fracture toughness do not influence the rate of propagation. Figures 13 and 14 show that crack propagation occurs both along and across primary alpha boundaries. Hence, it seems reasonable that crack propagation resistance cannot be increased unless the microstructure can be made to provide a less favorable path for crack propagation. Based on light microscopy, such a change seems to be difficult.

Artificial sea water reduces crack propagation resistance by a factor of about 2 to 3 and affects all microstructures in the same way. While no microstructural studies were done, it is apparent that the needle-like structure of the primary alpha grains in the beta-forged Ti-6Al-4V does not provide any preferred sites for stress corrosion in an artificial sea water environment. Fager and Spurr (8) have observed preferred crystallographic planes for crack propagation. These preferred paths were not detected in our limited study.

Low cycle fatigue crack propagation studies have been made on Ti-6Al-4V alloys at the Naval Research Labs where it was found that the crack growth rate from a 1/4-inch-long machined notch in fully reversed

bending could be expressed as a empirical relationship of the form

$$\Delta L / \Delta N = K (\epsilon_T)^n$$

where $\Delta L/\Delta N$ = crack propagation rate (in/cycle)

ϵ_T = total strain range

K = material constant $\approx 5 \times 10^{11}$ for Ti-6Al-4V

n = material constant = 8 for Ti-6Al-4V

The second stage crack growth data obtained for ϵ m = 0 and 0.9% strain range agrees well with this relationship as shown in Figure 15. Since the equation expressing the first and the second stage crack growth rates are similar for all materials, it is anticipated that with data from other strain levels first stage crack growth could also be adequately defined by an exponential strain dependent relationship of the form used for second stage crack growth.

Incorporation of a mean strain equal to half the strain range results in a much increased crack propagation rate. It is expected that the above empirical relationship can be modified to incorporate the effect of mean strain. The data obtained to date at the 0.9% strain level would indicate that a K of approximately 30 x 10^{11} would result in very good agreement for a mean strain equal to half of the strain range.

Crack growth rates were comparable despite the fact that beta-forged titanium had a higher fracture toughness as measured by K_{IC}. However, the beta-forged material would still be expected to retain an inherent advantage in the ability to sustain a longer critical crack prior to the onset of rapid tensile fracture in accordance with the relationship:

$$K_{IC} \simeq \sigma \sqrt{a_{CRIT}}$$

where K_{IC} = plane strain fracture toughness

σ = stress level

a_{crit} = critical crack length

Thus, the 20% increase in fracture toughness afforded by the beta-forged material should provide an approximately 40% increase in critical crack length at a given stress level. However, the alpha-beta forged material will sustain a greater total number of fatigue cycles because of its significant increase in crack initiation resistance. The benefit of the observed moderate increase in fracture toughness becomes secondary since compressor disks are removed from service well within the range of stable crack growth.

Conclusions

The following conclusions can be made concerning the low cycle fatigue behavior of beta and alpha-beta forged Ti-6Al-4V conventionally solution treated in the alpha-beta region and aged at 1300°F:

1) Beta-forged material has lower resistance to crack initiation than alpha-beta forged material by a factor of 2:1.

2) For the microstructures tested, beta-forged material shows no improvement in crack propagation resistance over alpha-beta forged material despite the higher fracture toughness of the beta-forged material.

3) Artificial sea water reduces the crack propagation resistance of all microstructures tested by a factor of 2 to 3.

4) Glass-bead peening increases the minimum crack initiation life of each microstructure tested by 2:1. Maximum initiation life remains the same.

5) Calculated life to crack initiation values based on the static tensile properties show good agreement with experimental results.

Acknowledgment

The authors wish to thank R. A. Sprague and C. E. Spaeth for their valuable contribution to program initiation and direction and to R. C. Boettner for advice and consultation. The authors also wish to express their thanks to R. M. Masci for conducting the tests described.

Table 1. Billet Material Chemistry and Processing Variables

BILLET MATERIAL

Average Chemistry

Al	V	C	H_2	N_2	O_2	Fe	Ti
6.48%	4.01	0.026	0.0032	0.017	0.136	0.07	Balance

Processing Variables

Forging Temperature

Microstructure	Block	Finish	Heat Treatment
50% primary alpha	1750°F	1750°F	1765°F(1hr)WQ+1300°F(2hrs) AC
50% primary alpha	1750°F	1750°F	1765°F(1hr)WQ+1300°F(2hrs) AC
10% primary alpha	1750°F	1750°F	1805°F(1hr)WQ+1300°F(2hrs) AC
10% primary alpha	1750°F	1750°F	1805°F(1hr)WQ+1300°F(2hrs) AC
Transformed beta	1775°F	1925°F	1775°F(1hr)WQ+1300°F(2hrs) AC
Transformed beta	1775°F	1925°F	1775°F(1hr)WQ+1300°F(2hrs) AC

Table 2. Room Temperature Tensile Properties and K_{IC} Values of Ti-6Al-4V

Microstructure	UTS (KSI)	0.2%YS (KSI)	0.02%YS (KSI)	Elong. (%)	R.A. (%)	K_{IC} (KSI$\sqrt{in}$)
50% primary alpha	150.4	140.6	128.5	16.5	33.5	74.5
10% primary alpha	155.5	144.5	133.6	13.9	29.2	81
Transformed beta	149.4	137.5	121.3	12.5	23.2	91
Ti-6Al-4V Spec.	130	120		10	25	

Table III. Low Cycle Fatigue Tests of Three Microstructures of Ti-6Al-4V

Microstructure	Stress Range	Cycles to 1st Indication	Cycles to 1/32" Crack	Cycles to Failure	Propagation Cycles
50% primary alpha	0-100 ksi	4,660	4,660	13,555	8,895
"	"	11,950	16,550	17,688	5,738
"	"	19,150	26,550	28,583	9,433
"	"	19,550	24,000	24,857	5,307
"	"	23,000	28,000	36,898	13,898
10% primary alpha	0-100 ksi	8,350	10,350	15,275	6,925
"	"	10,000	10,000	13,656	3,656
"	"	15,000	15,000	19,982	4,982
"	"	15,700	23,500	27,733	12,033
"	"	16,950	24,000	27,384	10,425
"	"	17,800	28,200	30,137	12,337
Transformed beta	0-100 ksi	9,000	11,000	20,398	11,398
"	"	9,000	14,000	18,550	9,550
"	"	13,300	20,800	24,342	11,042
"	"	13,300	13,300	20,555	7,255
"	"	19,050	19,050	23,748	4,698

Table IV. Machining Procedure for Surface of Ti-6Al-4V Bending Specimen

1. Hole 7/16" dia. to be drilled at 112 rpm .004" feed.
2. Bore hole from 0.438" to 0.452" dia. using boring tool at 112 rpm .004 feed.
3. Bore hole from 0.452" to 0.494" dia. using boring tool at 112 rpm .004 feed.
4. Semi-finish bore with boring tool to 0.494" dia. at 450 rpm 0.002" feed.
5. Finish bore to 0.500" dia. at 450 rpm 0.002" feed.
6. Hone at 425 rpm 10 psi pressure 80 strokes using HSU-4 stone.
7. Use PMC 9252 broaching oil. Cutting oil for above operations.
8. Remove burrs on holes; 0.005-0.010" x 45° chem. max. is permissible on holes.
9. Butterfly polish using 320 grit energy cloth, 1500 rpm.

Table V. Cycles to Crack Initiation for Various Microstructures

	Beta (XHX-110)	10% Primary Alpha (XHX-158)	50% Primary Alpha (XHX-154)
Group 1 Surface - As-machined	2000	4000	4000
	2000	5000	9000
	3000	6000	10000
	4000	10000	
	Beta (XHX-162)	**10% Primary Alpha (XHX-157)**	**50% Primary Alpha (XHX-153)**
Group 2 Surface - As-machined	2000	6000	4000
	3000	7000	7000
	4000	16000	8000
	4000		9000
	Beta (XHX-162)	**10% Primary Alpha (XHX-157)**	**50% Primary Alpha (XHX-153)**
Group 3 Surface - As-machined and Glass Bead Peened	4000	8000	9000
	4000	8000	9000
	4000	10000	9000

Table VI. First and Second Stage Crack Growth Rates (Microinches/Cycle)

50% Primary Alpha		10% Primary Alpha		Beta Forged	
First Stage	Second Stage	First Stage	Second Stage	First Stage	Second Stage
Air Environment Strain Range 0-0.9%					
---	120	---	140	6.8	---
6.3	120	9.0	100	9.0	185
11.1	160	12.0	130	8.8	135
				---	185
Aqueous Salt Environment Strain Range 0-0.9%					
16.7	360	21.0	520	23	360
19	440	19.0	520	28	440
		22.5	520	25	440
Air Environment Surface Glass Bead Peened Strain Range 0-0.9%					
7.5	200				
5.0	107				
1.25	130				
Air Environment Strain Range ±0.45% Fully Reversed Bending					
1.0	32	0.7	---	1.4	24
2.0	26	1.4	18	1.9	18

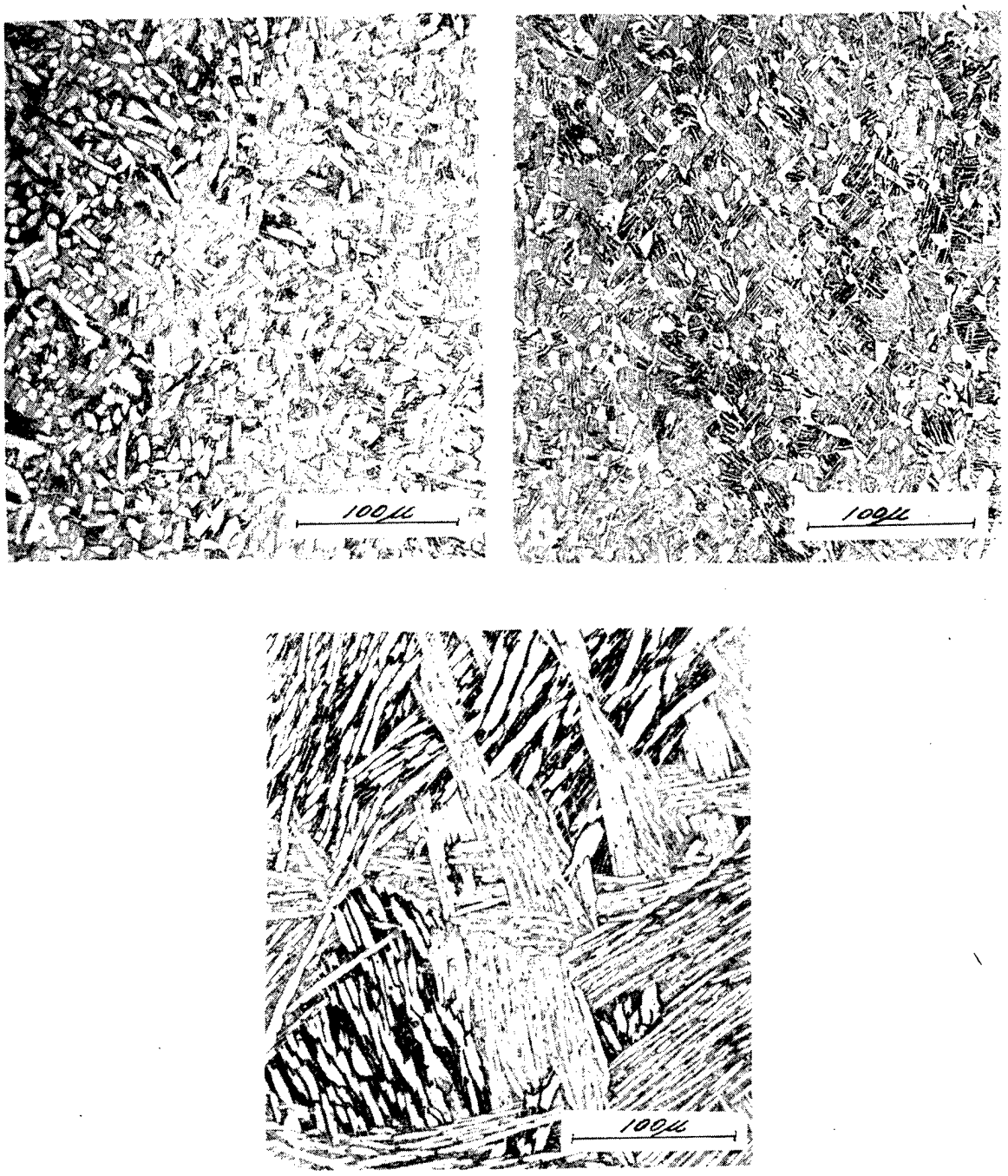

Fig. 1. Typical microstructures of Ti-6Al-4V specimens. Kroll's etch. 250X. (A) 50% primary alpha (B) 10% primary alpha (C) beta forged.

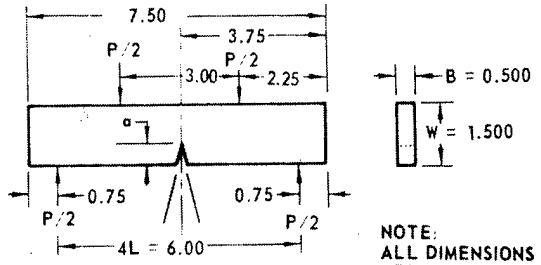

$$K = \frac{PL}{BW^{3/2}}\left[\left(\frac{1}{\pi\mu^2}\right)\left(34.7\frac{a}{W} - 55.2\left(\frac{a}{W}\right)^2 + 196\left(\frac{a}{W}\right)^3\right)\right]^{1/2}$$

Fig. 2. Four-point loaded notched bend specimen configuration.

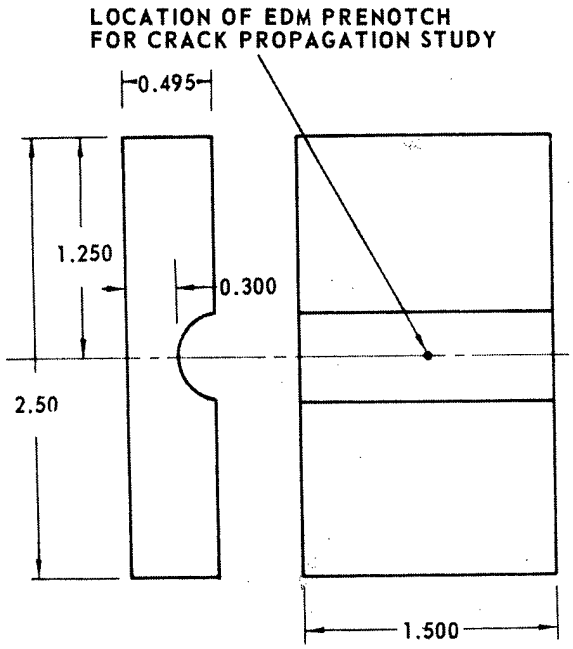

Fig. 3. Strain controlled bending test specimen.

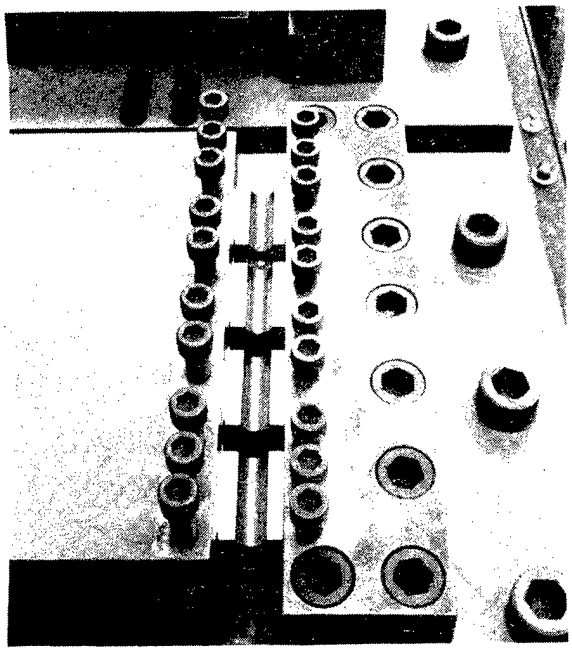

Fig. 4. Test rig and specimen.

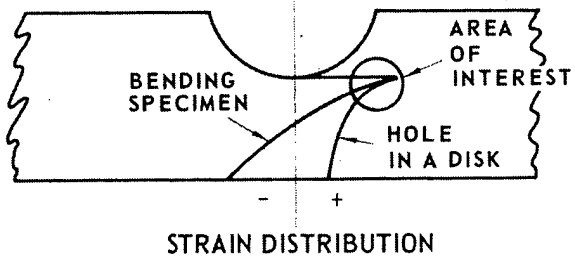

Fig. 5. Strain distribution for bending specimen vs. hole in a disk.

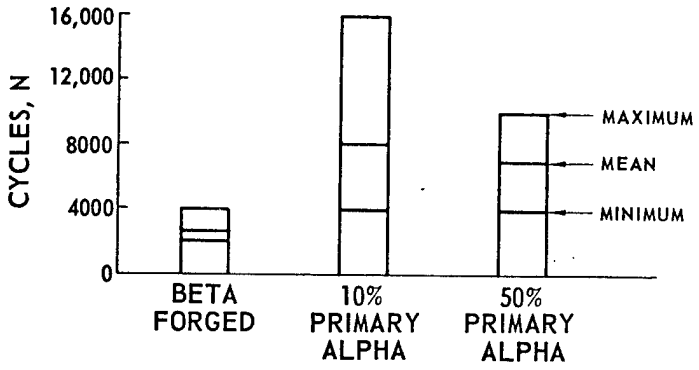

Fig. 6. Range of fatigue life for as-machined surface.

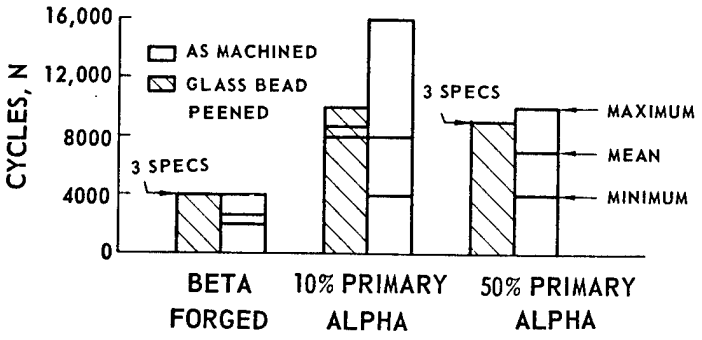

Fig. 7. Range of fatigue life for as-machined and glass bead peened surfaces.

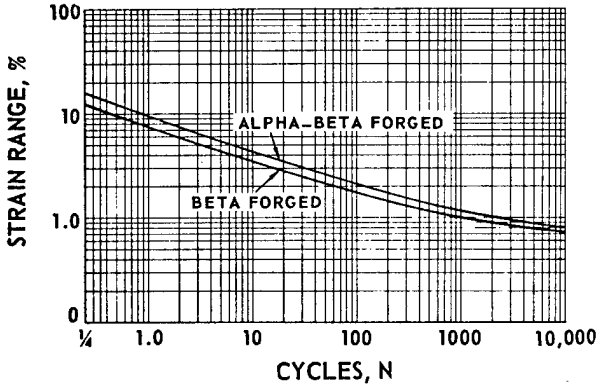

Fig. 8. Predicted fatigue curve for alpha-beta and beta forged Ti-6Al-4V based on static tensile properties.

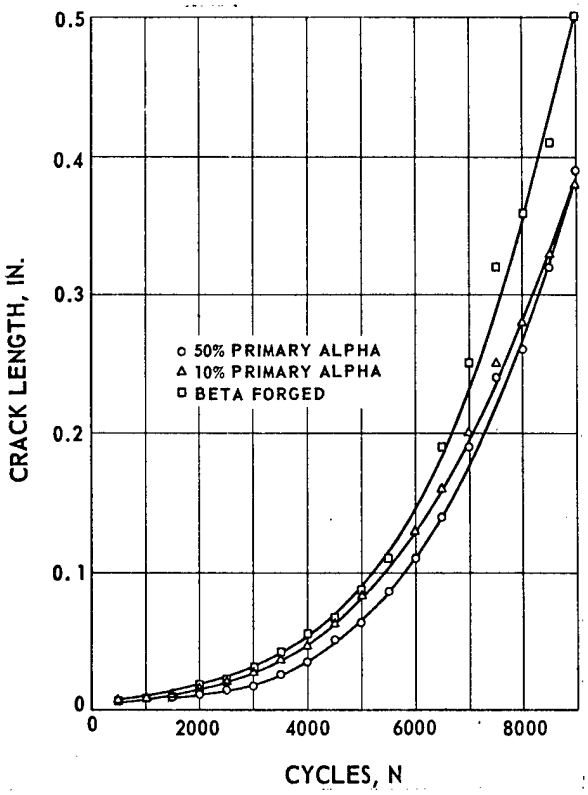

Fig. 9. Crack growth, EDM notched specimens tested in air, 0-0.9% strain range.

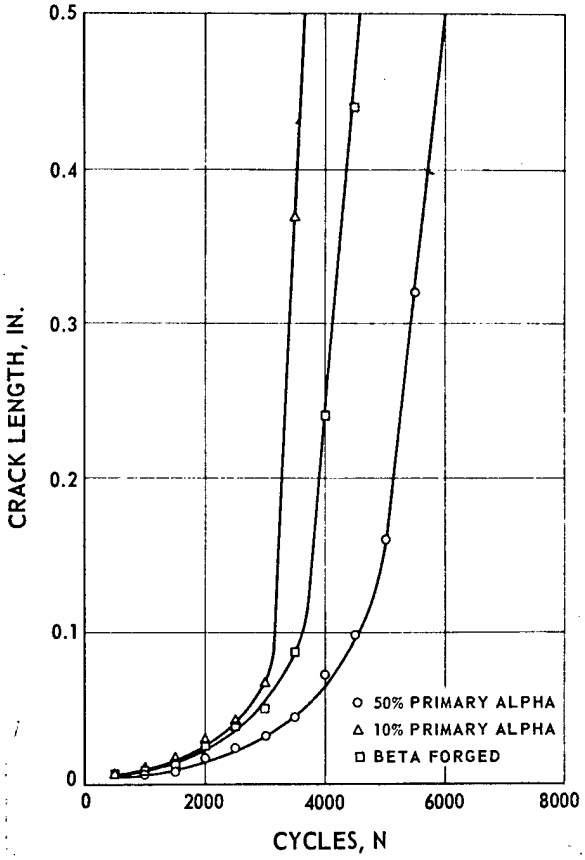

Fig. 10. Crack growth, EDM notched specimens tested in artificial sea water, 0-0.9% strain range.

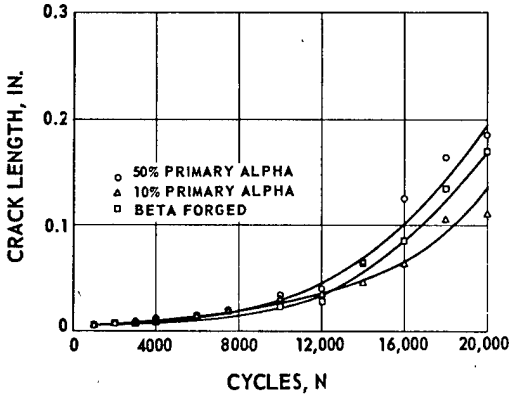

Fig. 11. Crack growth, EDM notched specimens tested in air, ±0.45% strain range.

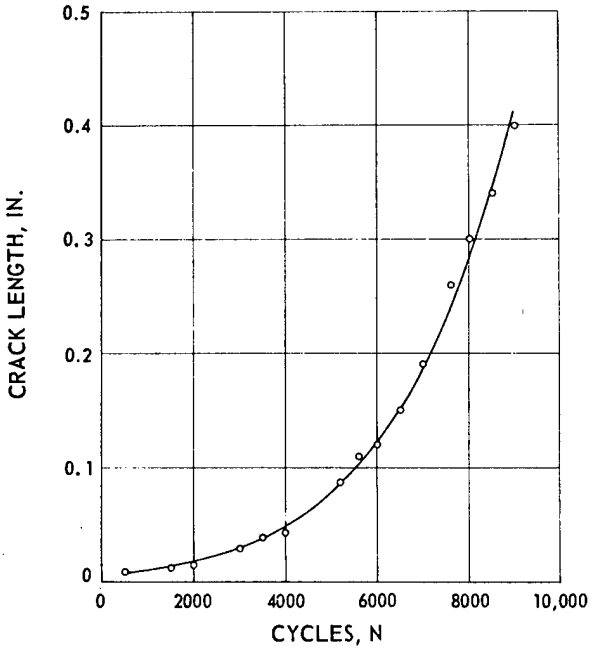

Fig. 12. Crack growth, EDM notched 50% primary alpha tested in air, 0-0.9% strain range, glass bead peened.

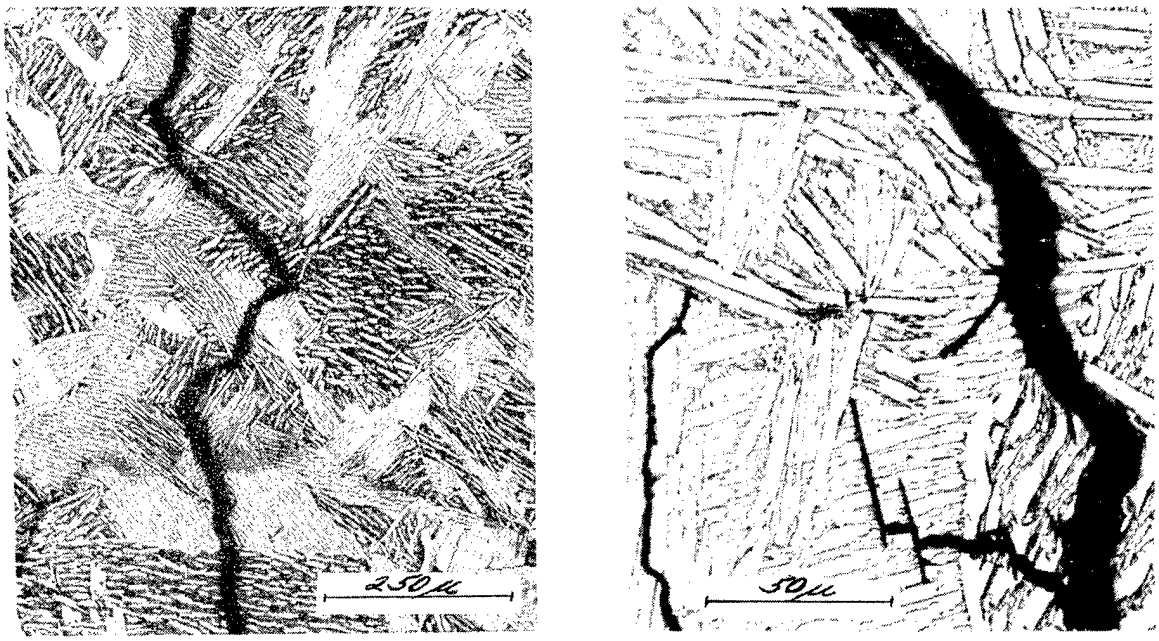

Fig. 13. Crack propagation in transformed beta microstructure (A) Crack moves across prior beta grains. 100X (B) Crack moves along and across primary alpha plates. 500X. Kroll's etch.

Fig. 14. Crack propagation in alpha-beta microstructure. Crack moves along and between primary alpha grains. Kroll's etch. 500X.

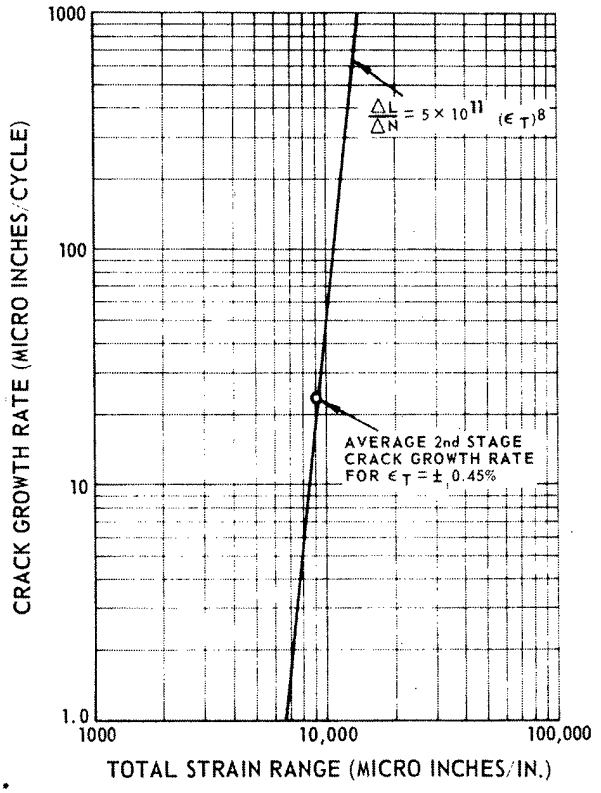

Fig. 15. Comparison of 2nd stage crack growth data with mathematical expression from Ref. 2.

REFERENCES - DMIC-73967

1. T. W. Crooker and E. A. Lange, Low Cycle Fatigue Crack Propagation Resistance of Materials for Large Welded Structures in Fatigue Crack Propagation, ASTM Special Technical Publication No. 415 (1967), p 94.

2. E. A. Lange, et al, Metallurgical Characteristics of High Strength Structural Materials, U.S. Naval Research Laboratory Report No. 6258, December 1964.

3. C. H. Wells and C. P. Sullivan, Low Cycle Fatigue Crack Initiation in Ti-6Al-4V P&WA Report, April 8, 1968 (Unpublished).

4. S. S. Manson, Fatigue: A Complex Subject - Some Simple Approximations Experimental Mechanics, 5 (1965).

5. L. F. Coffin, Jr., A Study of the Effects of Cyclic Thermal Stresses in Ductile Metals, Trans ASME, Vol. 76, 1954, pp 931-950.

6. J. G. Sessler and V. Weiss, Low Cycle Fatigue Damage in Pressure Vessel Materials, Journal Basic Engineering, December 1965, pp 539-547.

7. J. F. Tavernelli and L. F. Coffin, Jr., Experimental Support for Generalized Equation Predicting Low Cycle Fatigue, Journal Basic Engineering, December 1962, pp 533-541.

8. D. N. Fager and W. F. Spurr, Some Characteristics of Aqueous Stress Corrosion in Titanium Alloys, Trans ASM, 61, 1968, pp 283-291.